Cell cycle localization dynamics of mitochondrial DNA polymerase IC in African trypanosomes

Jeniffer Concepción-Acevedo, Jonathan C. Miller, Michael J. Boucher, and Michele M. Klingbeil*
Department of Microbiology, University of Massachusetts Amherst, Amherst, MA 01003

ABSTRACT ***Trypanosoma brucei*** **has a unique catenated mitochondrial DNA (mtDNA) network called kinetoplast DNA (kDNA). Replication of kDNA occurs once per cell cycle in near synchrony with nuclear S phase and requires the coordination of many proteins. Among these are three essential DNA polymerases (TbPOLIB, IC, and ID). Localization dynamics of these proteins with respect to kDNA replication stages and how they coordinate their functions during replication are not well understood. We previously demonstrated that TbPOLID undergoes dynamic localization changes that are coupled to kDNA replication events. Here, we report the localization of TbPOLIC, a second essential DNA polymerase, and demonstrate the accumulation of TbPOLIC foci at active kDNA replication sites (antipodal sites) during stage II of the kDNA duplication cycle. While TbPOLIC was undetectable by immunofluorescence during other cell cycle stages, steady-state protein levels measured by Western blot remained constant. TbPOLIC foci colocalized with the fraction of TbPOLID that localized to the antipodal sites. However, the partial colocalization of the two essential DNA polymerases suggests a highly dynamic environment at the antipodal sites to coordinate the trafficking of replication proteins during kDNA synthesis. These data indicate that cell cycle–dependent localization is a major regulatory mechanism for essential mtDNA polymerases during kDNA replication.**

Monitoring Editor
Thomas D. Fox
Cornell University

Received: Feb 20, 2018
Revised: Aug 10, 2018
Accepted: Aug 14, 2018

INTRODUCTION

Mitochondria are multifunctional organelles that maintain and express their own genome (mtDNA), which is organized as nucleoprotein assemblies called nucleoids. Mechanisms of mtDNA maintenance have gained wide interest because of their role in inherited diseases and aging (Schapira, 2012). Despite this renewed interest, there are still many unanswered fundamental questions surrounding inheritance, repair, regulation of copy number, and replication mechanisms of mtDNA. Some contributing features that have made answering these questions challenging include variation in mtDNA copy number among organisms and even within tissue types of the same organism, remodeling of nucleoid structure and composition in response to metabolic conditions, and importantly, no strict cell cycle control of organelle or nucleoid duplication (Kucej *et al.*, 2008; Spelbrink, 2010).

Trypanosoma brucei is the parasitic protist responsible for African sleeping sickness and is one of the earliest diverging eukaryotes with a bona fide mitochondrion. In contrast to most other eukaryotes, *T. brucei* has a single tubular mitochondrion containing a structurally complex mtDNA network known as kinetoplast DNA (kDNA), which is composed of topologically interlocked DNA minicircles and maxicircles. Each network contains ~5000 minicircles and 25 maxicircles and is condensed into a single nucleoid structure in vivo (Shlomai, 2004; Jensen and Englund, 2012). Maxicircles are homologous to mtDNA in other eukaryotes, encoding several subunits of the respiratory complex and mitochondrial rRNAs. Extensive RNA editing (insertion and/or deletion of uridine residues) of maxicircle transcripts is required to generate functional open reading frames (Aphasizhev and Aphasizheva, 2011). Minicircle-encoded gRNAs specify the sequence information for editing. Therefore, the

This article was published online ahead of print in MBoC in Press (http://www.molbiolcell.org/cgi/doi/10.1091/mbc.E18-02-0127) on August 22, 2018.

*Address correspondence to: Michele M. Klingbeil (klingbeil@microbio.umass.edu).

Abbreviations used: 3D, three-dimensional; bb, basal body; CHX, cycloheximide; DAPI, 4′,6-diamidino-2-phenylindole; dNTP, deoxyribonucleotide triphosphate; EM, electron microscopy; HA, hemagglutinin; HU, hydroxyurea; IF, immunofluorescence; kDNA, kinetoplast DNA; KFZ, kinetoflagellar zone; PBS, phosphate-buffered saline; Puro, puromycin; RNAi, RNA interference; SIM, structured illumination microscopy; TAC, tripartite attachment complex; TdT, terminal deoxynucleotidyl transferase; ULF, unilateral filament

information encoded within minicircles and maxicircles is fundamental for mitochondrial functions, and replication of both is thus essential for cell viability.

A hallmark of kDNA replication is the minicircle release and attachment mechanism, while maxicircles replicate catenated within the network (Sela *et al.*, 2008). Importantly, the kDNA network is replicated in near synchrony with nuclear S phase (Woodward and Gull, 1990). The current model for kDNA replication indicates a spatial and temporal separation of events. The early stages of minicircle replication (release, initiation, and synthesis) occur in the specialized region called the kinetoflagellar zone (KFZ) also known as the unilateral filament (ULF) region of the tripartite attachment complex (TAC) (Drew and Englund, 2001; Ogbadoyi *et al.*, 2003). Later stages, such as completion of synthesis, Okazaki fragment processing, and topoisomerase-mediated attachment of minicircle progeny, occur in two protein assemblies located at opposite poles of the network periphery (antipodal sites) (Melendy *et al.*, 1988; Ferguson *et al.*, 1994; Hines *et al.*, 2001). Minicircles and maxicircles replicate unidirectionally as theta structures and produce progeny with gaps. The minicircle progeny are attached to the network while still containing at least one gap. The network elongates, and after DNA content has doubled, the network divides into two daughter networks. Then, remaining gaps and nicks are repaired, and the TAC, a structure connecting the kDNA with the flagellar basal body (bb), mediates the segregation of progeny networks (Ogbadoyi *et al.*, 2003).

In striking contrast to the minimal required set of mammalian mtDNA replication enzymes (Korhonen *et al.*, 2004), trypanosome mitochondria harbor multiple enzymes with similar activities but nonredundant roles in kDNA maintenance. Among these are two primases (PRI1 and PRI2) related to those of large DNA viruses; two ligases (ligase kα and kβ), also related to viral sequences; two topoisomerases (type IA and type II); six PIF1-like helicases; and six DNA polymerases. PRI1 and PRI2 are essential for maxicircle and minicircle replication, respectively (Hines and Ray, 2010, 2011), while the ligases seal discontinuities (Downey *et al.*, 2005). Topoisomerase IA is essential for theta structure resolution, while topoisomerase II_{mt} ($TopoII_{mt}$) appears to have several roles, including attachment of minicircle progeny to the network and remodeling of the network during replication (Lindsay *et al.*, 2008; Scocca and Shapiro, 2008). Three of the PIF1-like helicases are essential for cell viability and kDNA maintenance and have roles ranging from minicircle (TbPIF1) and maxicircle replication (TbPIF2) to kDNA segregation (TbPIF8) (Liu *et al.*, 2009, 2010; Wang *et al.*, 2012). The *T. brucei* mtDNA polymerases belong to family A and family X, which contain replicative and repair enzymes, respectively. The family X enzymes, DNA polymerase (Pol) β and Pol β-PAK, are presumably involved in Okazaki fragment processing and filling the final gaps, respectively (Saxowsky *et al.*, 2003). The four family A Pols (TbPOLIA, IB, IC, and ID) are more similar to bacterial Pol I than to Pol γ, the sole mitochondrial replicative enzyme in other eukaryotes (Klingbeil *et al.*, 2002). Three of these (TbPOLIB, IC, and ID) are essential for *T. brucei* growth and kDNA replication in both life cycle stages (insect and bloodstream form) (Klingbeil *et al.*, 2002; Chandler *et al.*, 2008; Bruhn *et al.*, 2010, 2011). While POLIB and TbPOLID have demonstrated roles in minicircle replication, a precise role for TbPOLIC in kDNA maintenance has not been determined.

Initial localization studies of the three essential DNA Pols using peptide antibodies showed that TbPOLIB and TbPOLIC localized to the KFZ/ULF, while TbPOLID was distributed throughout the mitochondrial matrix (Klingbeil *et al.*, 2002). The matrix localization of TbPOLID suggested that this protein would need to redistribute to perform its essential role in kDNA replication. However, cell cycle dynamics were never analyzed. The tight link between bb duplication and kDNA synthesis allowed Gluenz and colleagues to describe five stages (I–V) of the kDNA duplication cycle (Gluenz *et al.*, 2011), and we demonstrated that changes in TbPOLID localization were coordinated with stages II and III of the kDNA duplication cycle (Concepción-Acevedo *et al.*, 2012). During these stages, TbPOLID concentrated as foci that colocalized with replicating minicircles at the antipodal sites. These data demonstrate that TbPOLID is available to perform its role in replication as a result of dynamic localization and represent a significant step toward understanding the spatiotemporal coordination of proteins during kDNA replication.

So far, three mechanisms have been proposed to regulate kDNA replication proteins and, as a result, kDNA replication events: 1) redox control of UMSBP binding to the minicircle origin sequence (Onn *et al.*, 2004), 2) *trans*-acting factors that regulate the mRNA stability of kDNA replication proteins during the cell cycle (Mittra *et al.*, 2003), and 3) proteolytic degradation of TbPIF2 by HslVU-like protease to control maxicircle copy number (Li *et al.*, 2008). Studies in the related kinetoplastid *Crithidia fasciculata* indicate that several kDNA replication proteins (Pol β, UMSBP, $TopoII_{mt}$, SSE1, and ligase kα) undergo localization changes during the cell cycle (Johnson and Englund, 1998; Engel and Ray, 1999; Abu-Elneel *et al.*, 2001; Sinha *et al.*, 2006). Additionally, a great majority of newly identified essential kDNA replication proteins appear to localize near the kDNA disk in only a fraction of cells in an asynchronous population, suggesting possible cell cycle localization. These observations in concert with TbPOLID redistribution data suggest that a dynamic change in protein localization is a potential mechanism to control kDNA replication.

In this study, we provide a comprehensive analysis of TbPOLIC localization. We demonstrate that TbPOLIC foci localize to the antipodal sites during stage II of the kDNA replication cycle and remain undetectable at other cell cycle stages. Proteolytic degradation is not involved in the regulation of TbPOLIC localization, as protein levels remain constant after inhibition of protein synthesis. Additionally, we demonstrate that TbPOLIC colocalizes with active kDNA replication sites as well as with a fraction of TbPOLID at the antipodal sites. Taken together, these data demonstrate that a second kDNA replication protein of *T. brucei* accumulates to the antipodal sites in a cell cycle–dependent manner and likely undergoes redistribution in order to perform its essential role in kDNA replication.

RESULTS

TbPOLIC has a cell cycle–dependent localization

Multiple DNA polymerases are involved in kDNA replication, but the mechanism by which these DNA polymerases are spatially and temporally coordinated during kDNA replication stages remains largely unknown. Previously, we demonstrated that TbPOLID undergoes dramatic changes in localization that are coupled to kDNA synthesis (Concepción-Acevedo *et al.*, 2012). We hypothesize that cell cycle–dependent localization of *T. brucei* mitochondrial DNA (mtDNA) polymerases provides a mechanism for spatial and temporal regulation during kDNA replication stages. The localization dynamics of TbPOLIC, an essential Pol I-like mtDNA polymerase that was previously detected in the KFZ (Klingbeil *et al.*, 2002), was examined in detail using an immunofluorescence (IF)-based approach. Key for this strategy is the TbIC-PTP cell line, in which one TbPOLIC allele was deleted and the other was fused to the PTP tag. POLIC-PTP was detected as discrete foci in a subpopulation of the cells in three clonal cell lines (unpublished data). Only data for clone P2C1

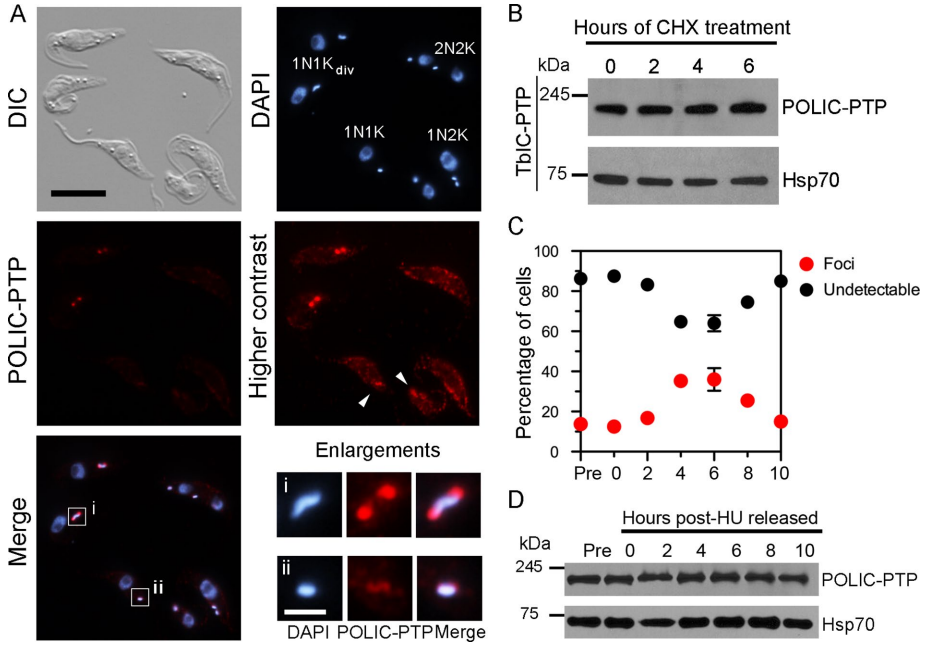

FIGURE 1: POLIC-PTP foci and protein levels. (A) Localization of POLIC-PTP in asynchronous TbIC-PTP cells. POLIC-PTP was detected using anti–protein A (red), and DNA was stained with DAPI (blue). Brightness and contrast of the POLIC-PTP images were adjusted in Adobe Photoshop to generate the higher-contrast panel. Arrowheads indicate cells with POLIC-PTP that was undetectable before adjustment. Rows i and ii, enlargements of the white boxes in the merged field. Scale bars: 10 μm (standard images) and 2 μm (enlarged images). (B) Western blot detection of POLIC-PTP (~200 kDa) and Hsp70 following CHX treatment. Cells were harvested every 2 h, and 5×10^6 cells were loaded into each well. (C) The percentages of POLIC-PTP foci–positive cells (red circles) and those with undetectable POLIC-PTP foci (black circles) during HU synchronization. Data are presented as the mean percent of 200 cells from two independent experiments. Error bars represent the variation range. (D) Western blot detection of POLIC-PTP during HU synchronization. Membrane was stripped and reprobed with anti-Hsp70.

are shown in this study (Figure 1A). Similar to TbPOLID localization (Concepción-Acevedo *et al.*, 2012), POLIC-PTP foci were always detected in close proximity to the kDNA disk and were mainly in cells with elongated kDNA structures, a hallmark of cells undergoing kDNA replication (1N1K$_{div}$ cells) (Figure 1A, and enlargement i) (Siegel *et al.*, 2008; Gluenz *et al.*, 2011). POLIC-PTP was undetectable by IF in cells with segregated networks (1N2K, 2N2K). Additionally, weak POLIC-PTP signal was detected in 1N1K cells only after image contrast was increased (Figure 1A, arrowheads in higher-contrast image and enlargement ii). In these cells, POLIC-PTP is diffuse near the kDNA network rather than concentrated as distinct foci adjacent to the kDNA disk as seen in 1N1K$_{div}$ cells (Figure 1A, enlargements i and ii), Similar observations (discrete foci and diffuse signal) were detected in a TbPOLIC-hemagglutinin (HA)-tagged cell line using anti-HA sera. POLIC-HA foci were present in 1N1K$_{div}$ cells, and a diffuse signal was only detected in 1N1K cells after image contrast was increased. Therefore, the TbPOLIC localization pattern is not due to the PTP tag. (Supplemental Figure 1, arrowheads in higher contrast and enlargement i).

The *T. brucei* mitochondrial protease HslVU (Li *et al.*, 2008) could be responsible for regulating TbPOLIC protein levels, explaining why the protein is undetectable by IF in a subset of cells. To determine whether TbPOLIC protein abundance is controlled by proteolytic degradation, we monitored POLIC-PTP protein levels after inhibiting protein synthesis with cycloheximide (CHX). POLIC-PTP and POLIC-HA protein levels remained unchanged during the 6 h CHX treatment, as did those of Hsp70 and TbPOLID, which are not regulated by TbHslVU. Cyc6-HA, a positive control for a degraded protein via the ubiquitin-proteasome pathway (Di Renzo *et al.*, 2016), rapidly declined within 2 h of CHX treatment (Figure 1B and Supplemental Figure 2) (Concepción-Acevedo *et al.*, 2012). These data demonstrate that TbPOLIC is a stable protein that is not regulated by proteolysis. The discrete POLIC-PTP foci appeared to accumulate in a cell cycle–dependent manner. Therefore, we monitored POLIC-PTP foci and protein levels at 2 h intervals following hydroxyurea (HU) synchronization using conditions that are known to partially inhibit DNA synthesis and lead to an accumulation of 1N2K cells (Chowdhury *et al.*, 2008). The presence and absence of POLIC-PTP foci were scored at the indicated times (Figure 1C). During HU treatment and immediately following release, a small percentage of cells (13%, Pre and 0) contained POLIC-PTP foci, while the majority had completed kDNA segregation (61%, 1N2K and 2N2K). Post-HU release (4 and 6 h), the percentage of 1N1K cells increased (62.5 and 85%, respectively) with a notable increase in POLIC-PTP foci (35% of cells) (Figure 1C). Consistent with the CHX data, no significant changes in POLIC-PTP protein levels were detected following HU synchronization (Figure 1D). Together, these data demonstrate that POLIC-PTP foci accumulate in a subset of 1N1K cells, while protein levels remain constant during the cell cycle.

TbPOLIC foci correlate with stage II of the kDNA duplication cycle

Maturation of the new bb occurs almost in synchrony with initiation of kDNA S phase in the transition from 1N1K to 1N1K$_{div}$, and the subsequent movement and separation of the bbs are critical for morphogenesis and kDNA segregation during the cell cycle (Sherwin and Gull, 1989; Woodward and Gull, 1990). The five-stage kDNA duplication cycle defined by Gluenz and coworkers clearly shows that kDNA replication and morphogenesis are intimately tied to bb dynamics (Gluenz *et al.*, 2011). To precisely determine when POLIC-PTP foci accumulate in certain stages of the kDNA duplication cycle, we used bb positioning and DNA staining as markers for cell cycle stages in asynchronous cells. Stage I cells had a unit-sized kinetoplast (1N1K), 1 bb/probasal body (pbb) pair, and no detectable POLIC-PTP foci (Figure 2, column i). Weak POLIC-PTP signal near the kDNA disk was observed only after the image contrast was increased (Figure 2B, column i, bottom panel). Stage IIa cells contained a single kDNA associated with two closely positioned bbs, indicating the transition to 1N1K$_{div}$ (Figure 2A, column ii), and POLIC-PTP was detected as a single focus (or two foci that cannot be easily resolved) located mainly in the KFZ/ULF (between the kDNA disk and bb) (Figure 2, B and C, column ii). Stage IIb cells had a dome-shaped kDNA, two bb/pbb pair (Figure 2A, columns iii and iv), and two POLIC-PTP foci situated at opposite sides of the kDNA disk (Figure 2, B and C, columns iii and iv). POLIC-PTP signal was also detected between foci, suggesting that the protein may move

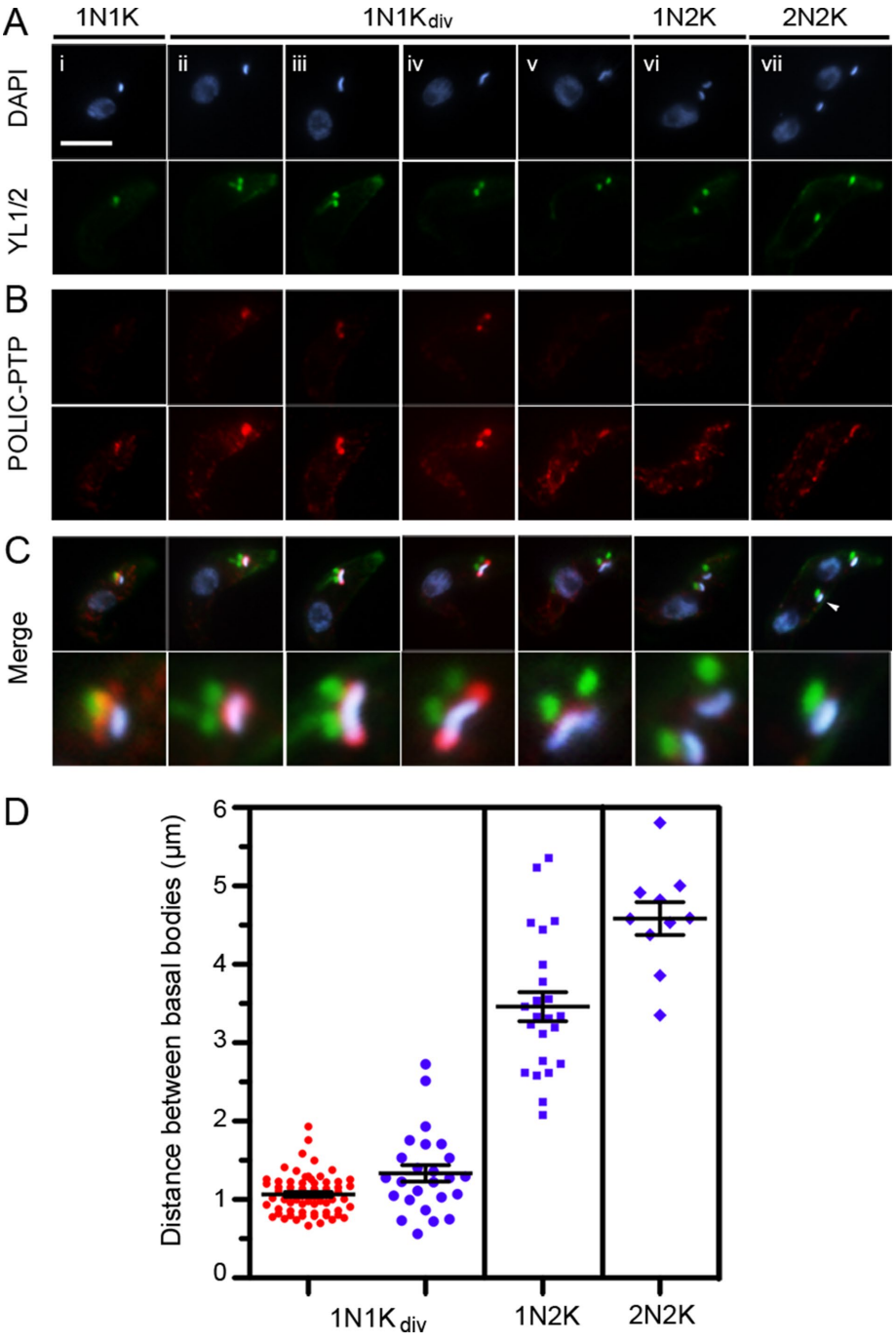

FIGURE 2: Localization of POLIC-PTP during the cell cycle. Representative cells from an unsynchronized population. TbIC-PTP cells were labeled with anti–protein A (red), YL1/2 (green), and DAPI (blue). (A) Detection of DNA (blue) and bb (green). Scale bar: 5 μm. (B) Detection of POLIC-PTP (red). Higher-contrast images are shown in the bottom row. (C) Merged images. Enlargements are shown in the bottom row. White arrowhead indicates enlarged area. (D) Inter-bb distances measured in 122 randomly selected cells with POLIC-PTP foci (red) or undetectable POLIC-PTP signal (blue). The average inter-bb distance of each group of cells is represented with a black bar. Error bars represent the SEM.

from the center to opposite sides of the kDNA disk (Figure 2B, column iii). Stage III cells contained two joined disks in a bilobe shape with two pairs of bb/pbb (Figure 2A, column v) and no detectable POLIC-PTP foci (Figure 2B, column v). Diffuse POLIC-PTP signal was detected near the kDNA after image contrast was increased (Figure 2, B and C, column v, bottom panel), but discrete foci were rarely detected, even at higher contrast. Stage IV and V cells contained two kinetoplasts, each associated with one of the two bbs that had separated farther apart from one another (Figure 2A, columns vi and vii), and POLIC-PTP was not detected (Figure 2, B and C, columns vi and vii). These data demonstrate that POLIC-PTP signal accumulates near the kDNA disk before stage II of the kDNA duplication cycle, is detectable as discrete foci during stages IIa and b, and then dissipates during stage III.

To quantitatively analyze when POLIC-PTP foci are detected within the kDNA duplication cycle, we measured the inter-bb distance in 122 randomly selected individual cells that were later grouped based on their karyotype and presence or absence of POLIC-PTP foci (Figure 2D, red and blue, respectively). Cells with obvious discrete POLIC-PTP foci had a minimum inter-bb distance of 0.66 μm and a maximum distance of 1.75 μm (Figure 2D). The mean bb distance of POLIC-PTP foci-positive 1N1K$_{div}$ cells was 1.1 μm (1.05 ± 0.02; $n = 64$) (Figure 2D, red) and 1.3 μm (1.33 ± 0.10; $n = 25$) for cells with undetectable foci (Figure 2D, 1N1K$_{div}$, blue). Discrete POLIC-PTP foci were never detected once cells reached an inter-bb distance ≥2 μm (stage IV) or in cells with a single bb. Together, these data indicate that POLIC-PTP foci detection is tightly linked to stage II of the kDNA duplication cycle.

Relationship of TbPOLIC localization with the TAC

TAC102 is a core protein of the TAC that is essential for proper kDNA segregation. The protein is detected throughout the cell cycle in the ULF zone and is assembled de novo into the TAC shortly after bb duplication (Trikin *et al.*, 2016). Electron microscopy (EM) cytochemistry defined inner and outer ULF domains (Gluenz *et al.*, 2007). It is possible that subdomains exist within the ULF zone for protein localization; one that occupies replication processes and others that occupy structural or other related processes. Although the precise role of TbPOLIC in kDNA maintenance is not known, the presence of ancillary DNA (mislocalized kinetoplast-derived DNA; Miyahira and Dvorak, 1994) during TbPOLIC RNA interference (RNAi) suggests a role in kDNA segregation. To investigate whether POLIC-PTP colocalizes with a known ULF marker TAC102, we used high-resolution structured illumination microscopy (SIM).

TAC102 signal was always detected in the ULF zone, closely resembling the previously published pattern (Trikin *et al.*, 2016), and

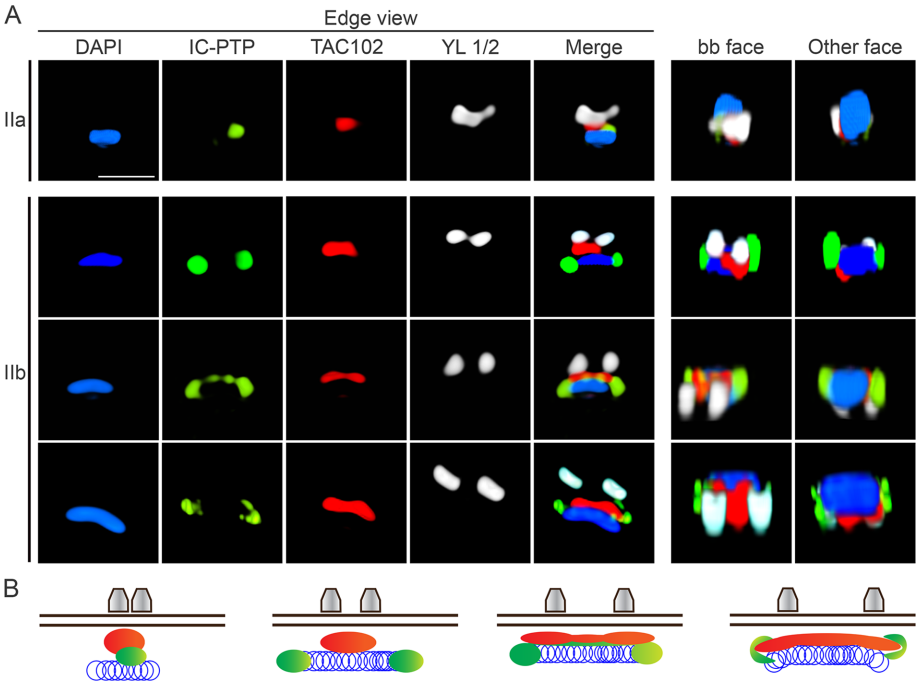

FIGURE 3: Three-dimensional SIM imaging of POLIC-PTP, TAC102, and basal bodies. TbIC-PTP cells were labeled with anti–protein A (green), anti-TAC102 (red), YL1/2 (white), and DAPI (blue). More than 20 cells were analyzed by 3D-SIM at each stage. Scale bar: 5 μm. (A) Representative images of POLIC-PTP, TAC102, and bb localization at stage IIa and stage IIb of kDNA replication. (B) Schematic model of localization of POLIC-PTP (green), TAC102 (red), and YL1/2 (gray) during stages IIa and IIb of kDNA replication. Videos of each representative image can be found in the Supplemental Material.

POLIC-PTP signal was detected only during kDNA synthesis phases, as described earlier. In three-dimensional (3D) reconstructions of cells at stage IIa or IIb of the kDNA duplication cycle, POLIC-PTP and TAC102 signals rarely overlapped with representative cells shown in Figure 3, the Supplemental Videos, and linear intensity profiles (Supplemental Figure 3). POLIC-PTP pattern varied the most at stage IIa, appearing as a single focus or more diffuse signal patterns that showed varying overlap with the TAC102 signal (Figure 3A and Supplemental Video 1). Three clearly defined localization patterns were detected for stage IIb cells that correlated with the transition through kDNA synthesis as measured by inter-bb distance (Figure 3A): POLIC-PTP foci localized only to the antipodal sites with no TAC102 overlap (Supplemental Video 2); POLIC-PTP signal appeared mainly at the antipodal sites with signal detected between the foci in the ULF that overlapped with TAC102 (Supplemental Video 3); and POLIC-PTP signal started to become less focused, taking on a crescent shape that localized adjacent to TAC102 in the ULF zone (Supplemental Video 4). These data demonstrate that the great majority of POLIC-PTP signal does not overlap with TAC102 signal even when both proteins localize to the KFZ/ULF zone (Figure 3B).

TbPOLIC foci colocalize with newly synthesized DNA at the antipodal sites

In the current model, free minicircles undergo theta structure replication in the KFZ/ULF zone, and their progeny undergo Okazaki fragment processing at the antipodal sites. Here, minicircle progeny containing at least one gap accumulate during kDNA replication and can be detected with terminal deoxynucleotidyl transferase (TdT) and a fluorescent deoxyribonucleotide triphosphate (dNTP) providing a marker for the antipodal sites (Guilbride and Englund, 1998; Liu *et al.*, 2005). EM analyses indicate that stage IIa cells already contain antipodal sites, indicating minicircle replication is proceeding (Gluenz *et al.*, 2011). To further define the localization of POLIC-PTP foci and the relationship with replicating minicircles, we used TdT labeling. Previously described early, late, and post–TdT-labeled cells were detected (Figure 4A). The 1N1K cells contained nonreplicating kDNA networks were TdT negative, and POLIC-PTP foci were not detected (Figure 4A, 1N1K). Early kDNA replication stages are characterized by a strong TdT signal at the antipodal sites, indicating an accumulation of gapped minicircle intermediates and progeny (Figure 3A, $1N1K_{div}$, Early TdT). POLIC-PTP foci were detected in a subset of early TdT-positive cells and colocalized with the antipodal TdT signal (Figure 4A, $1N1K_{div}$, merge, enlarged inset). During later kDNA replication stages, gapped minicircle progeny reattached to the network and were detected as TdT signal throughout the kDNA network, and POLIC-PTP foci were no longer detected (Figure 4A, $1N1K_{div}$, Late TdT). A subset of these cells showed diffuse POLIC-PTP labeling in the kDNA disk after images were adjusted for a higher contrast (unpublished data). POLIC-PTP foci were never detected after network segregation (Figure 4A, 1N2K Post, 1N2K, and 2N2K TdT-negative).

To determine the percentage of TdT-positive cells that exhibited POLIC-PTP foci, we examined ≥300 cells from three independent TdT-labeling experiments. Individual cells were classified by the presence (red bar) or absence (blue bars) of POLIC-PTP foci and by their karyotype. The 1N1K cells with no TdT signal and no obvious POLIC-PTP foci (Figure 4B, 1N1K, blue bar) represented 34% of the total population (34.0 ± 3.05; $N = 3$). TdT-positive cells with a single kinetoplast represented 44% of the total population, in agreement with previous data (Concepción-Acevedo *et al.*, 2012). POLIC-PTP foci were detected in a subset of the $1N1K_{div}$ TdT-positive cells (Figure 4B, $1N1K_{div}$, red bar) and represented 26% (25.6 ± 2.33; $N = 3$) of the total population. TdT-positive cells with no detectable POLIC-PTP foci (Figure 4B, $1N1K_{div}$, blue bar) represented 18% (18.3 ± 2.33; $N = 3$) of the total population. POLIC-PTP foci were never detected in 1N2K (11.6 ± 0.33; $N = 3$) or 2N2K (7.0 ± 1.52; $N = 3$) cells (Figure 4B).

To obtain further evidence that POLIC-PTP foci are present at the antipodal sites during kDNA replication, we incubated cells with the thymidine analogue BrdU and used IF microscopy with anti-BrdU to visualize the newly synthesized DNA. Only a subset of 1N1K cells were BrdU-positive (Figure 4C, rows i–iv, green), while 1N2K and 2N2K were always BrdU negative, as previously described (Gluenz *et al.*, 2011). During early kDNA replication stages, newly synthesized DNA was detected at the antipodal sites (Figure 4C, rows i and ii). In these cells, a portion of the POLIC-PTP foci (red) colocalized with newly replicated DNA (Figure 4C, rows i and ii). During later kDNA replication stages, the newly replicated molecules were distributed through the kDNA network, and the nuclear DNA was BrdU-positive, indicating initial S phase (Figure 4C, rows iii and iv). Only a subset of the double BrdU-positive cells contained POLIC-PTP foci,

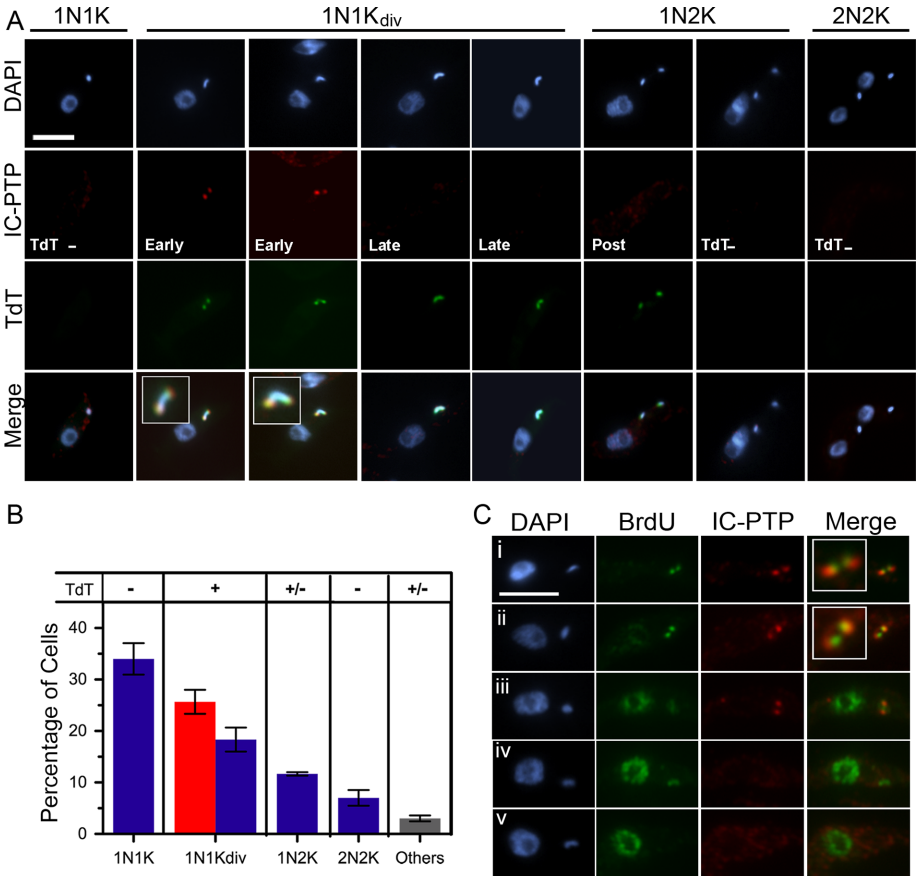

FIGURE 4: Localization of POLIC-PTP with respect to TdT and BrdU labeling. (A) Localization of POLIC-PTP (red) following in situ TdT labeling (green). Representative images for TdT-labeling patterns are shown (TdT–, Early, Late, and Post). Enlargements in the merged row correspond to those cells that displayed POLIC-PTP and TdT colocalization (yellow) at the antipodal sites. Scale bar: 5 μm. (B) Distribution of POLIC-PTP foci in unsynchronized TdT-labeled cells. Individual cells were classified based on kDNA morphology and the presence (red) or absence (blue) of POLIC-PTP foci. Others (gray bar) included cells with abnormal karyotypes, including multinucleated cells and zoids. More than 300 cells were analyzed in each experiment. Error bars correspond to the SEM from three separate experiments. (C) POLIC-PTP localization (red) following metabolic labeling of newly synthesized DNA. Representative images for BrdU-labeling patterns are shown (green). Enlargements in the merged column correspond to cells that displayed POLIC-PTP and BrdU colocalization (yellow) at the antipodal sites. Scale bar: 5 μm.

and we differentiated them based on kDNA morphology. Cells with a dome-shaped kinetoplast contained discrete POLIC-PTP foci (Figure 4C, row iii), while cells with a bilobed kinetoplast (two joined disks) had no detectable POLIC-PTP foci (Figure 4C, row iv). Cells that were BrdU-positive only for the nucleus had completed kDNA replication and did not exhibit discrete POLIC-PTP foci (Figure 4C, row v). This is in agreement with the earlier data defining POLIC-PTP foci during stage IIa of the duplication cycle (Figure 2). Notably, these data demonstrate that POLIC-PTP foci are associated with sites of newly synthesized DNA only during early kDNA replication stages.

TbPOLIC and TbPOLID foci colocalize at the antipodal sites during kDNA S phase

The antipodal sites are two protein-rich regions to which several proteins with differing enzymatic activities and functions localize (Ferguson *et al.*, 1994). Distinct subdomains may exist to coordinate activities. Okazaki fragment processing enzymes SSE1 and Pol β appear to colocalize (Engel and Ray, 1999), while TopoII$_{mt}$ and Lig kβ partially colocalize, suggesting that the latter two enzymes could occupy different antipodal site subdomains (Downey *et al.*, 2005). However, little is known about the spatiotemporal coordination of proteins during kDNA replication stages.

TbPOLID localizes to the antipodal sites only during kDNA S phase, and in this study, we have established that POLIC-PTP has antipodal localization during stage IIa. To investigate whether these two essential mtDNA polymerases might colocalize and to define spatiotemporal coordination within the kDNA replication cycle, we generated a cell line coexpressing TbPOLIC-HA and POLID-PTP to monitor protein localization by IF. We determined the kDNA replication status–based (early and late kDNA S phase) kDNA morphology. POLID-PTP (green) localized throughout the mitochondrial matrix and as discrete foci at the antipodal sites, as previously described (Concepción-Acevedo *et al.*, 2012) (Figure 5).

Accumulation of POLID-PTP foci was detected very early in kDNA replication (Figure 5, POLID-PTP, arrow). In these cells, POLIC-HA foci (red) were undetectable (Figure 5, POLIC-HA). However, weak POLIC-HA signal was detected after image contrast was increased (Supplemental Figure 4). As the kDNA replicated and assumed a more dome-shaped structure (Figure 5, enlargement ii, 1N1K$_{div}$ cells), POLID-PTP and POLIC-HA foci colocalized (Figure 5, merge and enlargement i). As the kDNA proceeds through replication (bilobed shape) (Figure 5, enlargement ii, top), POLIC-HA and POLID-PTP only partially colocalized (Figure 5, enlargement ii, bottom). The POLID-PTP signal was less organized and began to diffuse throughout the mitochondrial matrix. Cells at later stages of kDNA replication had no detectable POLIC-HA, but a fraction of POLID-PTP remained diffuse around the kDNA network (Figure 5, POLID-PTP, arrowhead). Finally, we analyzed 12 randomly selected fields ($n = 150$ cells) to determine the percentage of cells that exhibited POLIC-HA and POLID-PTP colocalization (precise and partial), using the colocalization finder plug-in from ImageJ. The two DNA polymerases colocalized in 17% of the cells analyzed, similar to the percentage of cells with individual foci in an unsynchronized population. Importantly, the two essential Pol I-like DNA polymerases, TbPOLIC and TbPOLID, appear to colocalize during early stages of kDNA replication.

Depletion of TbPOLID causes a reduction in POLIC-PTP foci-positive cells

Localization of one DNA polymerase could depend on the localization of another. To explore whether TbPOLID depletion affects POLIC-PTP localization, we generated a single-expresser POLIC-PTP cell line in 29-13 cells to also induce *TbPOLID* RNAi (TbIC-PTP/SLID). Tetracycline induction of the intramolecular *TbPOLID*-specific

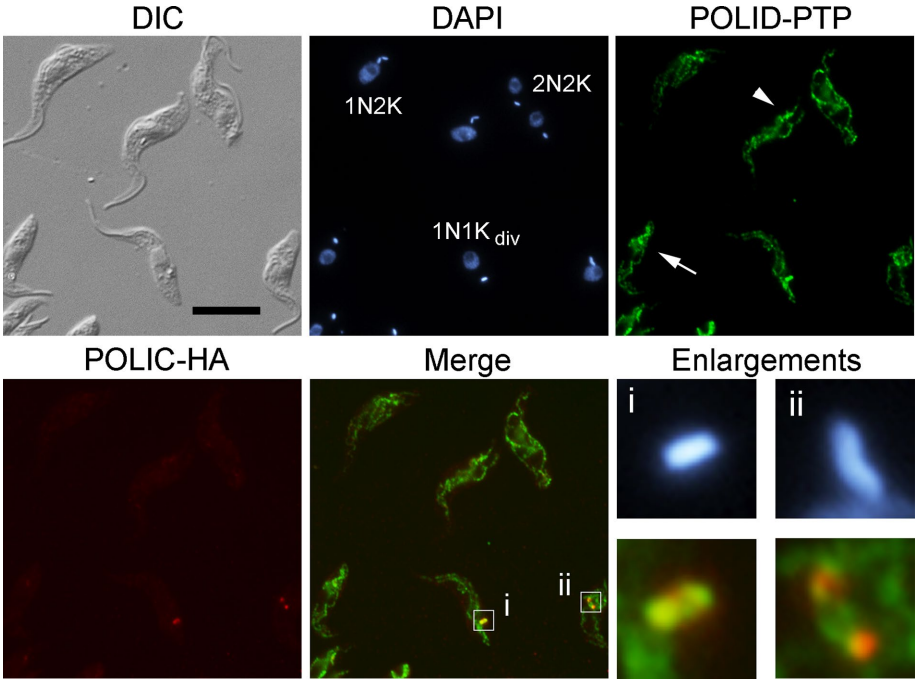

FIGURE 5: Colocalization of POLIC-HA and POLID-PTP. POLID-PTP (green) and POLIC-HA (red) were detected in TbID-PTP/POLIC-HA cells. Multiple karyotypes are indicated in DAPI-stained cells (blue). Arrow and arrowhead in POLID-PTP field indicate those 1N1K$_{div}$ cells that were positive for POLID-PTP foci and negative for POLIC-PTP detection. Columns i and ii are enlargements of the areas indicated by the white squares in the merge field. Scale bar: 10 μm.

stem-loop dsRNA resulted in growth inhibition starting at day 4 that persisted through the 8-day induction, in agreement with previous *TbPOLID* silencing (Figure 6A) (Chandler *et al.*, 2008). Quantitative PCR analysis revealed a 55% reduction of *TbPOLID* mRNA at 2 d postinduction with no significant changes in the mRNA levels for the two other essential mitochondrial Pols (*TbPOLIB* and *TbPOLIC*) (Figure 6B). For assessment of the effects of TbPOLID depletion on kDNA networks, uninduced and induced TbIC-PTP/SLID cells were 4′,6-diamidino-2-phenylindole (DAPI)-stained and examined by fluorescence microscopy to score the size of the kDNA network (200 cells per time point) (Figure 6C). The percentage of cells with a normal-sized kDNA network declined during the course of the induction, while the percentage of cells containing a small network and no kDNA increased to 20 and 72%, respectively by day 8. The kinetics of kDNA loss in TbIC-PTP/SLID cells was similar to those previously reported (Figure 6C).

We also evaluated the effects of *TbPOLID* RNAi on the accumulation of gapped minicircles at the antipodal sites and on the presence or absence of POLIC-PTP foci. Uninduced and induced (days 4 and 8) cells were labeled with DAPI, anti–protein A, and TdT. Early, late, and post–TdT-labeled cells were detected in the uninduced population (Figure 6, D and E; 30% were TdT positive), and POLIC-PTP foci colocalized with gapped minicircles at the antipodal sites as described in Figure 3 (Figure 6E, day 0). After 4 d of *TbPOLID* silencing, TdT-positive cells decreased to 9% of the population (Figure 6D). POLIC-PTP foci were present only in TdT-positive cells (Figure 6E), and the percentage of cells with POLIC-PTP foci decreased from 42 to 12% (unpublished data). Nearly all cells were TdT negative and lacked POLIC-PTP foci after 8 d of *TbPOLID* RNAi (Figure 6, D and E). These data suggest that accumulation and assembly of POLIC-PTP foci to the site of replication are dependent on TbPOLID expression and kDNA replication.

TbPOLID knockdown alters TbPOLIC protein levels

Although mRNA levels of *TbPOLIC* were not significantly altered, we investigated whether POLIC-PTP protein levels were affected by *TbPOLID* depletion. The protein levels of TbPOLIC and other mitochondrial proteins (trypanosome alternative oxidase [TAO] and mtHsp70) were monitored during *TbPOLID* RNAi from three separate experiments (Figure 7A). A representative experiment is shown in Figure 7A. The intensities of each band were quantified using ImageJ and were normalized using β-tubulin signal (Figure 7B). We detected a consistent downward trend of POLIC-PTP protein levels during *TbPOLID* silencing ($n = 3$). When a paired two-tailed t test was applied, day 4 (mean = 77.9, p value = 0.036) and day 8 (mean = 64.5, p = value 0.001) displayed a statistically significant decrease. After 8 d of *TbPOLID* RNAi, mitochondrial proteins (TAO, mtHsp70, and TbPOLIC) were differentially affected, but only POLIC-PTP protein levels consistently decreased (35% reduction) (Figure 7, A and B). We never detected proteolytic processing of POLIC-PTP or PTP tag (18.9 kDa) during *TbPOLID* silencing (Figure 7A). Here we demonstrate that POLIC-PTP protein levels are affected following *TbPOLID* silencing.

DISCUSSION

Nearly 30 kDNA replication proteins have been characterized at the single-protein level and associated with specific replication stages (Jensen and Englund, 2012). The interactions of these proteins and their spatiotemporal localizations during the cell cycle remain largely unexplored. Given the number of proteins reported to localize at the antipodal sites, we hypothesized that cell cycle localization might be a mechanism by which to coordinate subsets of replication proteins within the five stages of the kDNA duplication cycle. Our localization studies of a second essential mtDNA polymerase indicate that TbPOLIC transiently accumulates at the antipodal sites in cells that are undergoing kDNA replication, closely following the POLID-PTP foci pattern. We used epifluorescence to detect POLIC-PTP foci in a subset of 1N1K$_{div}$ cells (TdT positive, early) that localized to the antipodal sites during stage II of the kDNA duplication cycle (Figures 2 and 4). In contrast to TbPOLID, POLIC-PTP was not detected by IF in the mitochondrial matrix (Figures 1 and 2) and was undetected at other cell cycle stages, similar to the reported localizations of *T. brucei* mitochondrial Pol β and *C. fasciculata* SSE1 (Johnson and Englund, 1998; Engel and Ray, 1999; Saxowsky *et al.*, 2003). TbPOLIC steady-state protein levels during HU synchronization remained constant, indicating that change in protein abundance was not the reason for the undetected IF signal. The periodic detection of POLIC-PTP may be due to partially exposed epitopes in response to induced conformational changes during cell cycle progression. Alternatively, POLIC-PTP may only be detected when TbPOLIC local concentrations increase near the kDNA disk. In support of the latter possibility, we detected a diffuse POLIC-PTP signal in 1N1K cells after image contrast was increased (Figure 1A, arrowheads). The signal

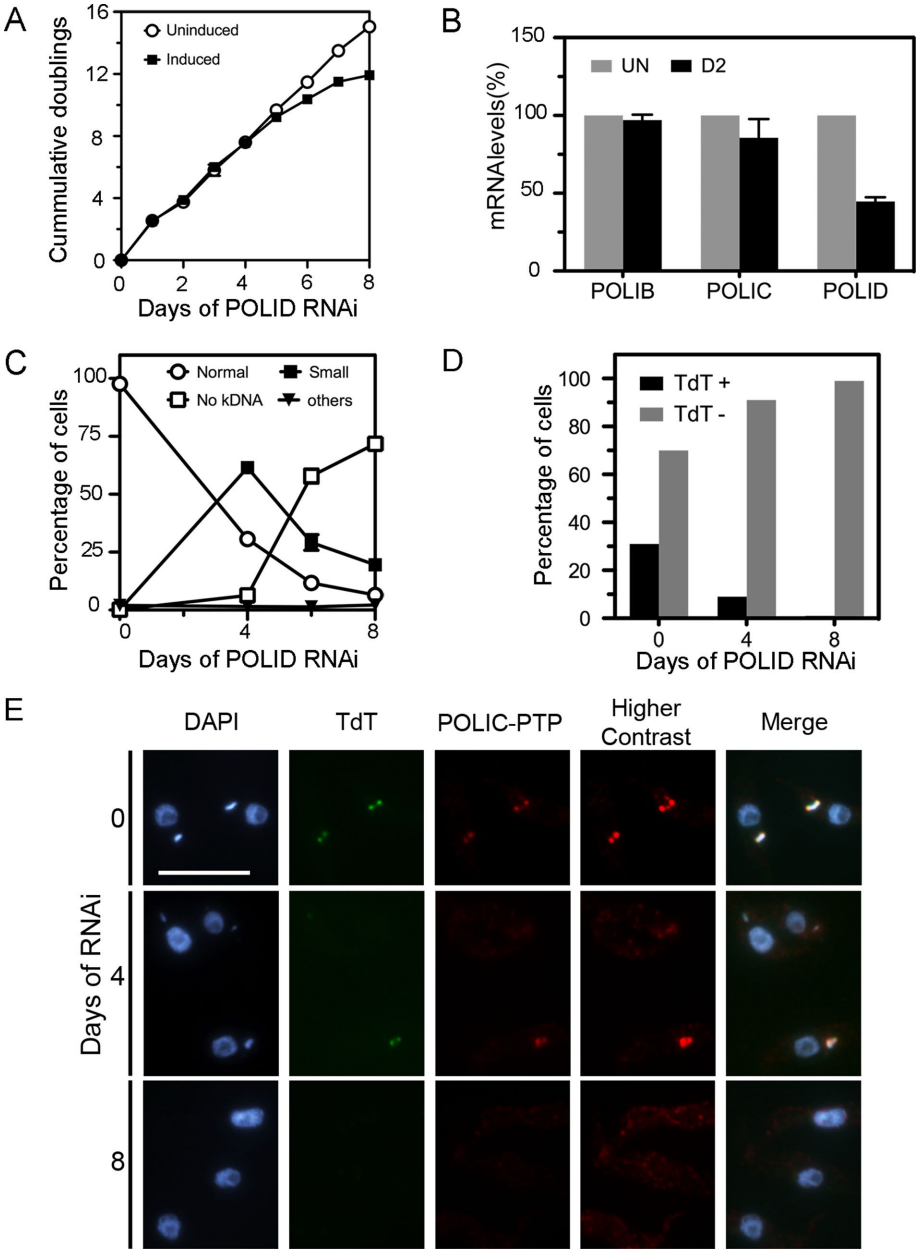

FIGURE 6: Effect of *TbPOLID* silencing on POLIC-PTP localization. (A) TbIC-PTP/SLID clonal cell line P1F3 was grown in the absence (open circles) or presence (filled squares) of tetracycline (1 µg/ml) to express the *TbPOLID* stem-loop dsRNA. Cell density was plotted as a function of cumulative doublings. Values represent the mean of four independent RNAi experiments. (B) Steady-state mRNA levels of *TbPOLIB*, *TbPOLIC*, and *TbPOLID* following 2 d (D2) of *TbPOLID* RNAi were analyzed by qRT-PCR using *GAPDH* as an internal control. Values represent the mean from three separate experiments. (C) Kinetics of kDNA loss. DAPI-stained cells (200 cells per time point) were scored for normal-sized kDNA (open circles), small kDNA (filled squares), or no kDNA (open squares). Others (filled triangles) represent cells with abnormal karyotypes. Values represent the mean from three independent experiments. Error bars represent the SEM. (D) Quantification of TdT-positive cells after 4 and 8 d of *TbPOLID* silencing (200 cells per time point). (E) Detection of POLIC-PTP (red) and TdT-positive cells (green) during *TbPOLID* silencing. DAPI-stained DNA is shown in blue. Representative images are shown. Scale bar: 10 µm.

concentrated between the kDNA disk and the flagellar bb or as a single elongated zone possibly representing two unresolvable foci (Figure 2C, columns i and ii, merge). Diffuse POLIC-PTP signal was detected before initiation of kDNA replication (single bb) or at very early stages (two closely spaced bbs), and resembled the previously reported TbPOLIC localization (Klingbeil *et al.*, 2002). These observations were consistent whether TbPOLIC was fused to a PTP or an HA tag, indicating that the localization patterns were not tag specific (Figure 1 and Supplemental Figure 1).

Consistent with a role in kDNA replication, a fraction of POLIC-PTP foci also colocalized with BrdU-positive antipodal sites (kDNA synthesis) (Figure 4C). On the basis of the patterns of POLIC-PTP signal (epifluorescence and SIM images), one could speculate that low levels of TbPOLIC are required in the KFZ at very early stages of kDNA replication. Then, as minicircles accumulate at the antipodal sites, a majority of the TbPOLIC molecules accumulate as foci at the antipodal sites. Localization of TbPOLIC to both regions (KFZ and antipodal sites) in a cell cycle–dependent manner could indicate multiple roles for TbPOLIC in the kDNA duplication cycle.

The increased resolution of SIM provided a more refined localization pattern for TbPOLIC with respect to a known ULF zone marker, TAC102 (Figure 3). During early kDNA replication (stage IIa), TbPOLIC may transiently interact with TAC102 or other TAC proteins to facilitate TbPOLIC activity. As kDNA synthesis proceeds (stage IIb), the TbPOLIC association with newly synthesized DNA at the antipodal sites appears to shift back to the KFZ/ULF zone, but not with TAC102 association, suggesting that subcomplexes of proteins likely exist in the KFZ/ULF zone. Previously, RNAi of *TbPOLIC* resulted in smaller kDNA networks, perturbation of minicircle replication, and ancillary DNA in ~12% of the cells (Klingbeil *et al.*, 2002). Accumulation of ancillary DNA (small extra kDNA mislocalized to the anterior of the cell) is associated with kDNA segregation defects for TAC102 (Trikin *et al.*, 2016) and PNT1, a cysteine peptidase (Grewal *et al.*, 2016), which supports the hypothesis that TbPOLIC may have multiple roles.

There are three DNA polymerases that localize to the antipodal sites (Pol β, TbPOLID, and now TbPOLIC). Although we could not coimmunoprecipitate POLIC-HA and POLID-PTP, by using the coexpressing cell line, we demonstrated that the two proteins colocalized with partial and precise overlap during early stages of kDNA replication (Figure 5, enlargement i). However, at later stages (Figure 5, enlargement ii, dome-shaped kDNA disk), POLIC-HA was below the level of detection and was only visible in cells after image contrast was increased (Figure 1), while TbPOLID was clearly detected as a diffuse signal that localized to the kDNA disk region (Figure 5, arrow and arrowhead). The

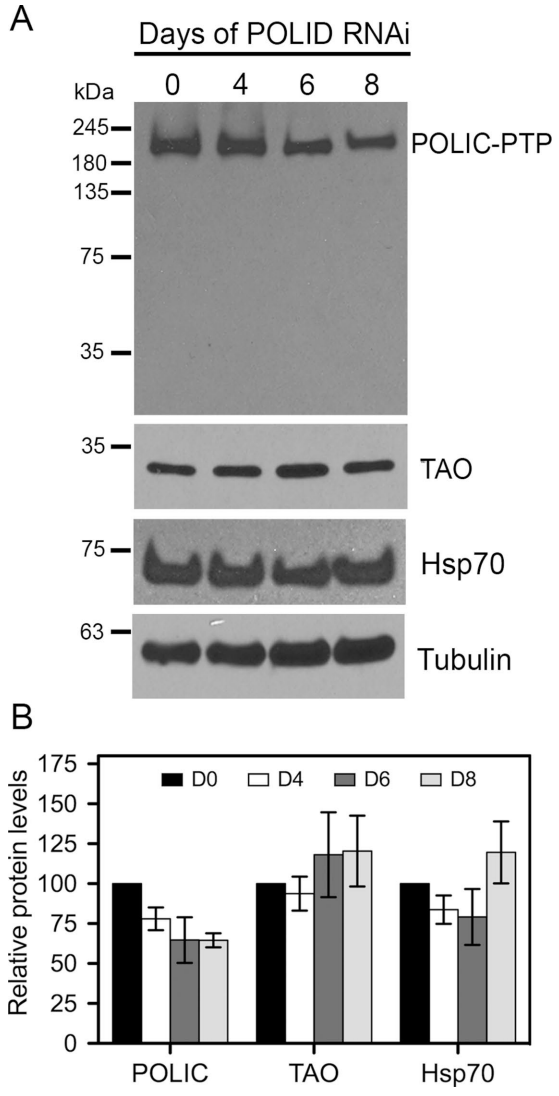

FIGURE 7: POLIC-PTP protein levels following *TbPOLID* silencing. (A) Western blot detection of POLIC-PTP, trypanosome alternative oxidase (TAO), and Hsp70 during *TbPOLID* RNAi. Cells were harvested at indicated times, and 5×10^6 cells were loaded into each lane. The membrane was probed with antibodies against each individual protein. (B) Quantification of the relative protein levels during *TbPOLID* RNAi. Values were normalized against tubulin, and relative protein levels were averaged from three independent experiments. Error bars represent the SEM.

stoichiometry of TbPOLIC and TbPOLID at the antipodal sites remains unknown. TbPOLID could be more abundant than TbPOLIC, thus allowing us to monitor TbPOLID accumulation at earlier stages of kDNA replication. We hypothesize that both proteins arrive and exit the antipodal sites at about the same time, but that there is a difference in the number of TbPOLIC and TbPOLID molecules recruited.

To evaluate whether TbPOLID depletion impacts TbPOLIC antipodal site localization, we silenced *TbPOLID* via RNAi in a POLIC-PTP single expressor cell line. Previously, we demonstrated that *TbPOLID* silencing resulted in growth inhibition, kDNA loss, and a parallel decline in covalently closed (unreplicated) and nicked/gapped (replicated) minicircles (Chandler *et al.*, 2008). *TbPOLID* silencing in this new cell line was consistent with the previously reported RNAi phenotype (Figure 6). Furthermore, we demonstrated that *TbPOLID* silencing caused a rapid decline (day 4) in gapped/replicating minicircles at the antipodal sites, indicating that minicircle replication was impaired (Figure 6, D and E), as is POLIC-PTP localization to the antipodal sites (Figure 6E). POLIC-PTP was never detected in cells with small kDNA and no kDNA. TbPOLIC localization to the antipodal sites appeared to depend on TbPOLID and kDNA replication. We cannot rule out the possibilities that loss of POLIC-PTP after *TbPOLID* RNAi was due directly or indirectly to a TbPOLID-POLIC-PTP interaction or due to loss of the kDNA network. So far, we have not been able to identify TbPOLIC or TbPOLID interacting partners through several approaches, which suggests that these cell cycle interactions are transient.

In other eukaryotes, mtDNA maintenance, transcription, and translation are under proteolytic control (Koppen and Langer, 2007). For example, *Drosophila* Lon protease regulates transcription by degrading the mitochondrial transcription factor A, which is essential for mitochondrial transcription and mtDNA packaging (Matsushima *et al.*, 2010). A Lon protease homologue has not been annotated in the *T. brucei* genome (Berriman *et al.*, 2005). However, a bacterial-like HslVU protease controls minicircle and maxicircle copy number by degrading the master regulators that participate in kDNA replication (Li *et al.*, 2008). RNAi demonstrated that TbPIF2 helicase is an HslVU substrate and controls maxicircle synthesis (Liu *et al.*, 2009). So far, a minicircle regulator has not been identified. HslVU does not appear to play a role in the transient accumulation of TbPOLIC foci. Levels of TbPOLIC protein and two other kDNA replication proteins with antipodal site localization, TbPOLID (Concepción-Acevedo *et al.*, 2012) and Pol β (Johnson and Englund, 1998), do not change when protein synthesis is inhibited or during hydroxyurea synchronization (Figure 1B and Supplemental Figure 2). Together, these data imply that alternative mechanisms regulate the cell cycle–dependent localizations of kDNA replication proteins.

Thus far, the mechanism(s) governing dynamic antipodal site localization is unknown. The antipodal sites could represent structural features that act as a landing pad for proteins at the various stages of kDNA replication. Binding affinities and interactions with structural elements or companion proteins could be regulated by posttranslational modifications like phosphorylation. However, phosphoproteome studies in *T. brucei* revealed no phosphopeptides corresponding to any of the mtDNA polymerases (Nett *et al.*, 2009; Urbaniak *et al.*, 2013). Other posttranslational modifications (methylation, palmitoylation, acetylation) are also important for regulating protein function and localization. Protein arginine methylation has evolved as an important regulatory factor for a number of cellular processes, including RNA processing, transcription, and subcellular localization (Bedford and Clarke, 2009). The first comprehensive survey of mitochondrial arginine methylproteins was completed in *T. brucei* and identified TbPOLIC as one of several arginine-methylated kDNA-associated proteins (Fisk *et al.*, 2013). Arginine methylation status of TbPOLIC may affect dynamic localization. Alternatively, TbPOLIC's enzymatic activity may be regulated by arginine methylation such that only methylated TbPOLIC participates in kDNA replication and localizes to the antipodal sites. In mammals, arginine methylation of DNA Pol β enhances polymerase activity by increasing DNA-binding affinity and binding to proliferating cell nuclear antigen (El-Andaloussi *et al.*, 2006, 2007). Further studies are necessary to determine the physiological significance of TbPOLIC methylation and any potential roles in dynamic localization.

Our findings confirm that spatiotemporal localization of kDNA replication proteins is an additional mechanism for regulating kDNA maintenance. Given the topological complexity and the predicted

large number of proteins needed to maintain the catenated kDNA network, it is not surprising that trypanosomes have evolved multiple mechanisms for coordinating and regulating kDNA replication proteins. An interesting question raised by these results is whether mtDNA replication in other model organisms is regulated by dynamic localization of nucleoid proteins. While dynamic localization has been proposed as a mechanism to regulate mammalian and yeast mtDNA replication, the dynamics of mitochondrial nucleoids and associated proteins remain poorly understood. This important process is more easily visualized in trypanosomes, which replicate their mitochondrial genome once every cell cycle, thus making trypanosomes a good model system to study the dynamics of mtDNA replication proteins.

MATERIALS AND METHODS

For primer sequences, refer to Supplemental Table 1.

Plasmid construction

TbPOLIC knockout constructs. For generation of pKOPOLIC^{Puro}, a 430–base pair *TbPOLIC* 5′ UTR fragment was PCR amplified and ligated into *Xho*I and *Hin*dIII sites in the upstream polylinker of the pKO^{Puro} vector (Lamb *et al.*, 2001). Subsequently, a 448–base pair *TbPOLIC* 3′ UTR fragment was PCR amplified and ligated into *Spe*I and *Xba*I sites in the downstream polylinker portion of pKO^{Puro} to generate pKOPOLIC^{Puro}. The puromycin resistance cassette from pKOPOLIC^{Puro} was replaced with a blasticidin cassette (*Asc*I/*Pac*I fragment) from pKO^{BSR} to generate pKOPOLIC^{BSR}.

PTP tag constructs. pPOLIC-PTP-PURO was generated as previously described (Bruhn *et al.*, 2010). For generation of pPOLIC-PTP-NEO, the *TbPOLIC* C-terminal coding sequence (2226 base pairs) was PCR amplified from the *T. brucei* genomic DNA and ligated into the *Apa*I and *Not*I restriction sites of the pC-PTP-NEO vector (Schimanski *et al.*, 2005). pPOLID-PTP-NEO was generated as previously described (Concepción-Acevedo *et al.*, 2012).

pMOPOLIC-HA-PURO. The *TbPOLIC* C-terminal coding sequence (1279 base pairs) and 3′ UTR region (996 base pairs) were PCR amplified from *T. brucei* genomic DNA and ligated into the pMOTagHA vector (Oberholzer *et al.*, 2006) to generate pMOPOLIC-HA-PURO.

Trypanosome growth

Procyclic *T. brucei* Lister 427 strain (doubling time, 9 h) was cultured as previously described (Concepción-Acevedo *et al.*, 2012), and the 29-13 strain (doubling time, 12.8 h) (Wirtz *et al.*, 1999) for RNAi was cultured as previously described (Chandler *et al.*, 2008).

Generation of cell lines

All cell lines were generated by elecroporation, as previously described (Chandler *et al.*, 2008).

TbIC-PTP. For POLIC-PTP–tagged cells, 427 wild-type cells were transfected with *Xho*I/*Xba*I-digested pKOPOLIC^{Puro} (15 µg). Stable transfectants were selected with 1 µg/ml puromycin (Puro) followed by limiting dilution as described previously (Klingbeil *et al.*, 2002). Southern blot analyses confirmed single-allele deletion in clonal cells. Clonal cell line P1A8 expressing a single *TbPOLIC* allele was then transfected with *Aat*I-linearized pPOLIC-PTP-NEO. POLICKO^{Puro}/IC-PTP cells were selected in media containing 1 µg/ml Puro and 50 µg/ml G418. After limiting dilution of POLICKO^{Puro}/IC-PTP cells, POLIC-PTP expression and localization, cell growth, and kDNA morphology were monitored in three individual clones (P2C2, P2A1, and P2C1). The average doubling times were 12 h, proper chromosomal integrations and no defects in kDNA morphology were detected (unpublished data). Data presented in this study correspond to clonal cell line POLICKO^{Puro}/IC-PTP P2C1, which we named TbIC-PTP.

TbID-PTP/ICHA. For generation of a cell line coexpressing POLIC-HA and POLID-PTP, POLID-PTP P2B7 cells (Concepción-Acevedo *et al.*, 2012) were transfected with *Pst*I/*Xba*I-digested pMOPOLIC-HA-PURO. TbID-PTP/ICHA cells were selected under 50 µg/ml G418 and 1 µg/ml puromycin and cloned by limiting dilution. Clone P2A5 was selected for our study, and we named this cell line TbID-PTP/ICHA.

RNAi cell lines: TbIC-PTP/SLID. The vector pSLID for *TbPOLID* RNAi was generated as previously reported (Chandler *et al.*, 2008). The pPOLIC-PTP-PURO construct was stably integrated into 29-13 cells as previously described (Bruhn *et al.*, 2010). This cell line was then transfected with *Not*I-linearized pSLID. Cells expressing POLIC-PTP and the *TbPOLID* stem-loop RNA were subsequently transfected with pKOPOLIC^{BSR} for knockout of *TbPOLIC* wild-type allele. Transfectants were selected with 15 µg/ml G418, 50 µg/ml hygromycin, 2.5 µg/ml phleomycin, 1 µg/ml puromycin, and 10 µg/ml blasticidin, followed by limiting dilution resulting in clonal cells expressing a single TbPOLIC PTP-tagged allele (POLIC-PTP/SLID/ICKO^{BSR}). Four clonal cell lines were evaluated for PTP expression by Western blotting, *TbPOLID* RNAi-silencing phenotype, and *TbPOLIC* single-allele knockout. Single knockout was confirmed by PCR amplification of POLIC-PTP/SLID/ICKO^{BSR} gDNA using primers that anneal to the 5′ end of the blasticidin cassette and the gene (Tb927.7.4000) immediately downstream of *TbPOLIC* to generate a 2.5-kb amplicon. The PCR product was sequenced for confirmation. Clonal cell line P1F3 was selected for this study and was named TbIC-PTP/SLID. RNAi was induced by adding 1 µg/ml tetracycline, and cell growth was monitored daily using the Z2 model Coulter Counter (Beckman Coulter).

In situ TdT labeling and quantification

In situ TdT labeling was described previously (Concepción-Acevedo *et al.*, 2012). TdT-labeled cells were quantified from three separate experiments (~900 total cells), and only intact cells as viewed by differential interference contrast were included in the analysis. Early and late TdT-positive cells were classified as 1N1K$_{div}$ cells, and TdT-negative cells were classified based on kDNA morphology identified by DAPI staining.

Immunofluorescence

Cells were harvested, washed, resuspended in phosphate-buffered saline (PBS), and adhered to poly-L-lysine (1:10)-coated slides for 5 min. Cells were then fixed in 4% paraformaldehyde (5 min) and washed three times (5 min) in PBS containing 0.1 M glycine (pH 7.4). Cells were permeabilized (0.1% Triton X-100 in PBS, 5 min) and washed in PBS three times (5 min). PTP-tagged proteins were detected with anti–protein A serum (1 h, Sigma, 1:3000) followed by Alexa Fluor 594 goat anti-rabbit (1 h, 1:250). POLIC-HA was detected with anti-HA 3F10 (1 h, Roche, 1:100) followed by Alexa Fluor 594 goat anti-rat (1 h, 1:100). Detection of bbs (YL1/2) and DNA (DAPI) was described previously (Concepción-Acevedo *et al.*, 2012). It should be noted that YL1/2 recognizes RP2, a protein that localizes to transitional fibers and is therefore a marker only for mature bbs (Andre *et al.*, 2014; Harmer *et al.*, 2017). Slides were then washed three times in PBS before being mounted in Vectashield (Vector Laboratories).

BrdU metabolic labeling

Mid–log phase cells were grown for 3 h in the presence of 50 μM BrdU and 50 μM deoxycytidine. Cells were fixed and permeabilized as described in the *Immunofluorescence* section. Cells were washed three times (5 min each) in PBS and incubated in 2 N HCl for 20 min at room temperature followed by three washes with PBS (5 min each) and blocking for 15 min using PBS containing 1% bovine serum albumin. For BrdU detection, slides were incubated with anti-BrdU (1 h, 1:50 clone PR-1, Alexa Fluor 488 conjugated, Millipore), washed in PBS + 0.1% Tween-20 (three times, 5 min each) incubated with secondary Alexa Fluor 488 goat anti-mouse (1 h, 1:50), and washed in PBS + 0.1% Tween-20. POLIC-PTP IF processing is described above.

Image acquisition and analysis

Microscope and software. Images were acquired with a Nikon Eclipse E600 microscope using a cooled CCD Spot-RT digital camera (Diagnostic Instruments) and a 100× Plan Fluor 1.30 (oil) objective. Image brightness and contrast were adjusted using Adobe Photoshop CS4.

Measurement of cell inter-bb distance. Cells were labeled with YL1/2 and anti–protein A for bb and POLIC-PTP detection, respectively. The inter-bb distance was measured in 122 cells from randomly selected fields using ImageJ software (http://imagej.nih.gov/ij). These cells were classified based on their kDNA morphology and the presence or absence of POLIC-PTP foci.

Colocalization analysis. An overlay of individual images acquired with the fluorescein isothiocyanate and tetramethylrhodamine isothiocyanate channel was done using ImageJ software. The colocalization Finder plug-in (http://rsb.info.nih.gov/ij/plugins/colocalization-finder.html) was used to identify overlapping pixels. We evaluated 157 cells to determine the percentage of cells that exhibited colocalization of POLIC-HA and POLID-PTP foci.

Three-dimensional SIM superresolution microscopy

Cells were processed for IF as described above with the following changes: anti–protein A (1:3000), YL1/2 (1:3000), TAC102 (1:10,000) and Alexa Fluor 647 goat α-mouse 1:1000, Alexa Fluor 488 goat α-rabbit 1:250, and Alexa Fluor 546 goat α-rat 1:400 secondary. Three-dimensional SIM (3D-SIM) was performed using a Nikon N-SIM E superresolution microscope equipped with an ORCA-Flash 4.0 sCMOS camera (Hamamatsu Photonics K.K.) and a CFI SR Apochromat TIRF 100× oil-objective (NA 1.49) lens. Z-stacks (6 μm, 240 nm thickness each) were acquired using the NIS-Elements Ar software. Image slices were reconstructed default software parameters and deconvolved using the Automatic method in NSIM modality. The 3D SIM videos display a top-down *x,y* coordinate view, then rotate along the *y*-axis to show three-dimensionality on the *x*-axis and *z*-axis, and finally along various transverse rotations for a complete 360° view. Videos were created using the Movie Maker option in the NIS-Elements Ar software at 50% volume zoom, high-resolution setting and were projected using alpha blending mode.

Statistics

Analysis of standard error of the mean (SEM) was performed using GraphPad Prism v. 5.00 for Mac OS X (GraphPad, San Diego, CA).

Western blotting

Cells were harvested and washed in PBS supplemented with protease inhibitor cocktail Set III (1:100) (CalBioChem). Cell lysate preparation, SDS–PAGE, and transfer were conducted as previously described (Concepción-Acevedo *et al.*, 2012). Membranes were incubated in 1% Roche blocking reagent (1 h) followed by incubation with antibodies diluted in 0.5% blocking reagent (1 h). Peroxidase–anti-peroxidase soluble complex reagent (1:2000, Sigma) was used for PTP-tag detection. Rat monoclonal anti-HA (1:1000, 3F10 clone, Roche) and goat anti-rat (1:1000, Sigma) were used for HA detection. For subsequent detections, membranes were stripped with 0.1 M glycine (pH 2.5, 15 min, 37°C), washed in TBS (0.1% Tween-20), and blocked and reprobed with one of the following primary/secondary antibody combinations: *C. fasciculata* anti-Hsp70 (1:5000) (Johnson and Englund, 1998)/chicken anti-rabbit (1:2000, Roche), *T. brucei* anti-Pol β (1:1000) (Saxowsky *et al.*, 2003)/goat anti-rat (1:5000) and anti-TAO (*T. brucei* alternative oxidase; 1:100) (Chaudhuri *et al.*, 1998)/goat anti-mouse (1:1000), and anti-tubulin (1:20,000, Sigma)/goat anti-mouse (1:1000). All secondary antibodies were horseradish peroxidase conjugated. Signal was detected with BM Chemiluminescence Western Blotting Substrate (POD) from Roche.

CHX treatment

TbIC-PTP cells and TbID-PTP/POLIC-HA–coexpressing cells were incubated for 6 h with 100 μg/ml CHX. Cells were harvested every 2 h for Western blot analysis (Concepción-Acevedo *et al.*, 2012).

Trypanosoma brucei 427 synchronization

Synchronization of *T. brucei* procyclic cells was performed as reported previously (Concepción-Acevedo *et al.*, 2012). Cells were quantified (200 cells per time point, $n = 2$) at the indicated times and classified based on the presence or absence of discrete POLIC-PTP foci as described above. POLIC-PTP protein levels were analyzed by Western blot.

RNA isolation and quantitative PCR

Total RNA was extracted from 5×10^7 cells using the TRIsol reagent (Ambion) according to the manufacturer's protocol. RNA (10 μg) was treated with 10 U (30 min at 37°C) of RNase-free DNase I (Bio-Rad) and subsequently cleaned using the RNA clean and concentrator kit (Zymo Research). The High Capacity cDNA Reverse Transcription Kit with RNase inhibitor (Ambion) and the Multi-Scribe Reverse Transcriptase were used to convert total RNA (500 ng) to cDNA. RT-PCR was performed in 10 μl reactions containing 1 μl cDNA template, 5 μl FastStart universal SYBR Green master (Rox) kit (Roche Diagnostics, Indianapolis, IN), 300 nM forward and reverse primers each, and nuclease-free water. Primers used for this analysis are listed in Supplemental Table 1. All data were normalized to *GAPDH*. The normalized values from induced samples were compared against uninduced controls for the relative expression levels of mRNA. Relative mRNA levels shown in Figure 5B are represented as means of three separate RNAi induction experiments.

ACKNOWLEDGMENTS

This work was partially supported by National Institutes of Health grant RO1AI0066279 to M.M.K. J.C.-A. was funded through the Northeast Alliance for Graduate Education and a Professoriate fellowship (National Science Foundation 0450339). J.C.M. received a research grant from the UMass Graduate School. We are grateful to Minu Chaudhuri for alternative oxidase antibody, Torsten Ochsenreiter for TAC102 antibodies, and Paul Englund for the mtHsp70 and Pol β antibodies. The superresolution microscopy data were gathered in the Light Microscopy Facility Nikon Center of Excellence at

the Institute for Applied Life Sciences, UMass Amherst, with support from the Massachusetts Life Sciences center. We also thank Aishwarya Swaminathan, Theresa A. Shapiro, Rahul Bakshi, James Morris, and Derrick Robinson for critiquing this article.

REFERENCES

Abu-Elneel K, Robinson DR, Drew ME, Englund PT, Shlomai J (2001). Intramitochondrial localization of universal minicircle sequence-binding protein, a trypanosomatid protein that binds kinetoplast minicircle replication origins. J Cell Biol 153, 725–734.

Andre J, Kerry L, Qi X, Hawkins E, Drizyte K, Ginger ML, McKean PG (2014). An alternative model for the role of RP2protein in flagellum assembly in the African trypanosome. J Biol Chem 289, 464–475.

Aphasizhev R, Aphasizheva I (2011). Uridine insertion/deletion editing in trypanosomes: a playground for RNA-guided information transfer. Wiley Interdiscip Rev RNA 2, 669–685.

Bedford MT, Clarke SG (2009). Protein arginine methylation in mammals: who, what, and why. Mol Cell 33, 1–13.

Berriman M, Ghedin E, Hertz-Fowler C, Blandin G, Renauld H, Bartholomeu DC, Lennard NJ, Caler E, Hamlin NE Haas B, *et al*. (2005). The genome of the African trypanosome *Trypanosoma brucei*. Science 309, 416–422.

Bruhn DF, Mozeleski B, Falkin L, Klingbeil MM (2010). Mitochondrial DNA polymerase POLIB is essential for minicircle DNA replication in African trypanosomes. Mol Microbiol 75, 1414–1425.

Bruhn DF, Sammartino MP, Klingbeil MM (2011). Three mitochondrial DNA polymerases are essential for kinetoplast DNA replication and survival of bloodstream form *Trypanosoma brucei*. Eukaryot Cell 10, 734–743.

Chandler J, Vandoros AV, Mozeleski B, Klingbeil MM (2008). Stem-loop silencing reveals that a third mitochondrial DNA polymerase, POLID, is required for kinetoplast DNA replication in trypanosomes. Eukaryot Cell 7, 2141–2146.

Chaudhuri M, Ajayi W, Hill GC (1998). Biochemical and molecular properties of the *Trypanosoma brucei* alternative oxidase. Mol Biochem Parasitol 95, 53–68.

Chowdhury AR, Zhao Z, Englund PT (2008). Effect of hydroxyurea on procyclic *Trypanosoma brucei*: an unconventional mechanism for achieving synchronous growth. Eukaryot Cell 7, 425–428.

Concepción-Acevedo J, Luo J, Klingbeil MM (2012). Dynamic localization of *Trypanosoma brucei* mitochondrial DNA polymerase ID. Eukaryot Cell 11, 844–855.

Di Renzo MA, Laverriere M, Schenkman S, Wehrendt DP, Tellez-Inon MT, Potenza M (2016). Characterization of *TcCYC6* from *Trypanosoma cruzi*, a gene with homology to mitotic cyclins. Parasit Int 65, 196–204.

Downey N, Hines JC, Sinha KM, Ray DS (2005). Mitochondrial DNA ligases of *Trypanosoma brucei*. Eukaryot Cell 4, 765–774.

Drew ME, Englund PT (2001). Intramitochondrial location and dynamics of *Crithidia fasciculat*a kinetoplast minicircle replication intermediates. J Cell Biol 153, 735–744.

El-Andaloussi N, Valovka T, Toueille M, Hassa PO, Gehrig P, Covic M, Hubscher U, Hottiger MO (2007). Methylation of DNA polymerase beta by protein arginine methyltransferase 1 regulates its binding to proliferating cell nuclear antigen. FASEB J 21, 26–34.

El-Andaloussi N, Valovka T, Toueille M, Steinacher R, Focke F, Gehrig P, Covic M, Hassa PO, Schar P, Hubscher U, *et al*. (2006). Arginine methylation regulates DNA polymerase beta. Mol Cell 22, 51–62.

Engel ML, Ray DS (1999). The kinetoplast structure-specific endonuclease I is related to the 5′ exo/endonuclease domain of bacterial DNA polymerase I and colocalizes with the kinetoplast topoisomerase II and DNA polymerase beta during replication. Proc Natl Acad Sci USA 96, 8455–8460.

Ferguson ML, Torri AF, Perez-Morga D, Ward DC, Englund PT (1994). Kinetoplast DNA replication: mechanistic differences between *Trypanosoma brucei* and *Crithidia fasciculata*. J Cell Biol 126, 631–639.

Fisk JC, Li J, Wang H, Aletta JM, Qu J, Read LK (2013). Proteomic analysis reveals diverse classes of arginine methylproteins in mitochondria of trypanosomes. Mol Cell Proteomics 12, 302–311.

Gluenz E, Povelones ML, Englund PT, Gull K, (2011). The kinetoplast duplication cycle in *Trypanosoma brucei* is orchestrated by cytoskeleton-mediated cell morphogenesis. Mol Cell Biol 31, 1012–1021.

Gluenz E, Shaw MK, Gull K (2007). Structural asymmetry and discrete nucleic acid subdomains in the *Trypanosoma brucei* kinetoplast. Mol Microbiol 64, 1529–1539.

Grewal JS, McLuskey K, Das D, Myburgh E, Wilkes J, Brown E, Lemgruber L, Gould MK, Burchmore RJ, Coombs GH, *et al*. (2016) PNT1 is a C11 cysteine peptidase essential for replication of the trypanosome kinetoplast. J Biol Chem 291, 9492–9500.

Guilbride DL, Englund PT (1998). The replication mechanism of kinetoplast DNA networks in several trypanosomatid species. J Cell Sci 111, 675–679.

Harmer J, Xi Q, Toniolo G, Patel A, Shaw H, Benson FE, Ginger ML, McKean PG (2017). Variation in basal body localisation and targeting of trypanosome RP2 and FOR20 proteins. Protist 168, 452–466.

Hines JC, Engel ML, Zhao H, Ray DS (2001). RNA primer removal and gap filling on a model minicircle replication intermediate. Mol Biochem Parasitol 115, 63–67.

Hines JC, Ray DS (2010). A mitochondrial DNA primase is essential for cell growth and kinetoplast DNA replication in *Trypanosoma brucei*. Mol Cell Biol 30, 1319–1328.

Hines JC, Ray DS (2011). A second mitochondrial DNA primase is essential for cell growth and kinetoplast minicircle DNA replication in *Trypanosoma brucei*. Eukaryot Cell 10, 445–454.

Jensen RE, Englund PT (2012). Network news: the duplication of kinetoplast DNA. Annu Rev Microbiol 66, 473–491.

Johnson CE, Englund PT (1998). Changes in organization of *Crithidia fasciculata* kinetoplast DNA replication proteins during the cell cycle. J Cell Biol 143, 911–919.

Klingbeil MM, Motyka SA, Englund PT (2002). Multiple mitochondrial DNA polymerases in *Trypanosoma brucei*. Mol Cell 10, 175–186.

Koppen M, Langer T (2007). Protein degradation within mitochondria: versatile activities of AAA proteases and other peptidases. Crit Rev Biochem Mol Biol 42, 221–242.

Korhonen JA, Pham XH, Pellegrini M, Falkenberg M (2004). Reconstitution of a minimal mtDNA replisome in vitro. EMBO J 23, 2423–2429.

Kucej M, Kucejova B, Subramanian R, Chen XJ, Butow RA (2008). Mitochondrial nucleoids undergo remodeling in response to metabolic cues. J Cell Sci 121, 1861–1868.

Lamb JR, Fu V, Wirtz E, Bangs JD (2001). Functional analysis of the trypanosomal AAA protein TbVCP with trans-dominant ATP hydrolysis mutants. J Biol Chem 276, 21512–21520.

Li Z, Lindsay ME, Motyka SA, Englund PT, Wang CC (2008). Identification of a bacterial-like HslVU protease in the mitochondria of *Trypanosoma brucei* and its role in mitochondrial DNA replication. PLoS Pathog 4, e1000048.

Lindsay ME, Gluenz E, Gull K, Englund PT (2008). A new function of *Trypanosoma brucei* mitochondrial topoisomerase II is to maintain kinetoplast DNA network topology. Mol Microbiol 70, 1465–1476.

Liu B, Wang J, Yaffe N, Lindsay ME, Zhao Z, Zick A, Shlomai J, Englund PT (2009). Trypanosomes have six mitochondrial DNA helicases with one controlling kinetoplast maxicircle replication. Mol Cell 35, 490–501.

Liu B, Yildirir G, Wang J, Tolun G, Griffith JD, Englund PT (2010). TbPIF1, a *Trypanosoma brucei* mitochondrial DNA helicase, is essential for kinetoplast minicircle replication. J Biol Chem 285, 7056–7066.

Liu Y, Motyka SA, Englund PT (2005). Effects of RNA interference of *Trypanosoma brucei* structure-specific endonuclease-I on kinetoplast DNA replication. J Biol Chem 280, 35513–35520.

Matsushima Y, Goto Y, Kaguni LS (2010). Mitochondrial Lon protease regulates mitochondrial DNA copy number and transcription by selective degradation of mitochondrial transcription factor A (TFAM). Proc Natl Acad Sci USA 107, 18410–18415.

Melendy T, Sheline C, Ray DS (1988). Localization of a type II DNA topoisomerase to two sites at the periphery of the kinetoplast DNA of *Crithidia fasciculata*. Cell 55, 1083–1088.

Mittra B, Sinha KM, Hines JC, Ray DS (2003). Presence of multiple mRNA cycling sequence element-binding proteins in *Crithidia fasciculata*. J Biol Chem 278, 26564–26571.

Miyahira Y, Dvorak JA (1994). Kinetoplastidae display naturally occurring ancillary DNA-containing structures. Mol Biochem Parasitol 65, 339–349.

Nett IR, Martin DM, Miranda-Saavedra D, Lamont D, Barber JD, Mehlert A, Ferguson MA (2009). The phosphoproteome of bloodstream form *Trypanosoma brucei*, causative agent of African sleeping sickness. Mol Cell Proteomics 8, 1527–1538.

Oberholzer M, Morand S, Kunz S, Seebeck T (2006). A vector series for rapid PCR-mediated C-terminal in situ tagging of Trypanosoma brucei genes. Mol Biochem Parasitol 145, 117–120.

Ogbadoyi EO, Robinson DR, Gull K, (2003). A high-order trans-membrane structural linkage is responsible for mitochondrial genome positioning and segregation by flagellar basal bodies in trypanosomes. Mol Biol Cell 14, 1769–1779.

Onn I, Milman-Shtepel N, Shlomai J (2004). Redox potential regulates binding of universal minicircle sequence binding protein at the kinetoplast DNA replication origin. Eukaryot Cell 3, 277–287.
Saxowsky TT, Choudhary G, Klingbeil MM, Englund PT (2003). *Trypanosoma brucei* has two distinct mitochondrial DNA polymerase beta enzymes. J Biol Chem 278, 49095–49101.
Schapira AH (2012). Mitochondrial diseases. Lancet 379, 1825–1834.
Schimanski B, Nguyen TN, Günzl A (2005). Highly efficient tandem affinity purification of trypanosome protein complexes based on a novel epitope combination. Eukaryot Cell 4, 1942–1950.
Scocca JR, Shapiro TA (2008) A mitochondrial topoisomerase IA essential for late theta structure resolution in African trypanosomes. Mol Microbiol 67, 820–829.
Sela D, Milman N, Kapeller I, Zick A, Bezalel R, Yaffe N, Shlomai J (2008). Unique characteristics of the kinetoplast DNA replication machinery provide potential drug targets in trypanosomatids. Adv Exp Med Biol 625, 9–21.
Sherwin T, Gull K (1989). The cell division cycle of *Trypanosoma brucei brucei*: timing of event markers and cytoskeletal modulations. Philos Trans R Soc Lond B Biol Sci 323, 573–588.
Shlomai J (2004). The structure and replication of kinetoplast DNA. Curr Mol Med 4, 623–647.
Siegel TN, Hekstra DR, Cross GA (2008). Analysis of the *Trypanosoma brucei* cell cycle by quantitative DAPI imaging. Mol Biochem Parasitol 160, 171–174.
Sinha KM, Hines JC, Ray DS (2006). Cell cycle-dependent localization and properties of a second mitochondrial DNA ligase in *Crithidia fasciculata*. Eukaryot Cell 5, 54–61.
Spelbrink JN (2010). Functional organization of mammalian mitochondrial DNA in nucleoids: history, recent developments, and future challenges. IUBMB Life 62, 19–32.
Trikin R, Doiron N, Hoffmann A, Haenni B, Jakob M, Schnaufer A, Schimanski B, Zuber B, Ochsenreiter T (2016). TAC102 is a novel component of the mitochondrial genome segregation machinery in trypanosomes. PLoS Pathog 12, e1005586.
Urbaniak MD, Martin D, Ferguson MA (2013) Global quantitative SILAC phosphoproteomics reveals differential phosphorylation is widespread between the procyclic and bloodstream form lifecycle stages of *Trypanosoma brucei*. J Proteome Res 12, 2233–2244.
Wang J, Englund PT, Jensen RE (2012).TbPIF8, a *Trypanosoma brucei* protein related to the yeast Pif1 helicase, is essential for cell viability and mitochondrial genome maintenance. Mol Microbiol 83, 471–485.
Wirtz E, Leal S, Ochatt C, Cross GA (1999). A tightly regulated inducible expression system for conditional gene knock-outs and dominant-negative genetics in Trypanosoma brucei. Mol Biochem Parasitol 99, 89–101.
Woodward R, Gull K (1990). Timing of nuclear and kinetoplast DNA replication and early morphological events in the cell cycle of *Trypanosoma brucei*. J Cell Sci 95, 49–57.